

Studying the properties of photonic quasi-crystals by the scaling convergence method

This article has been downloaded from IOPscience. Please scroll down to see the full text article.

2013 J. Phys. D: Appl. Phys. 46 145106

(<http://iopscience.iop.org/0022-3727/46/14/145106>)

View [the table of contents for this issue](#), or go to the [journal homepage](#) for more

Download details:

IP Address: 140.116.46.64

The article was downloaded on 15/03/2013 at 14:44

Please note that [terms and conditions apply](#).

Studying the properties of photonic quasi-crystals by the scaling convergence method

I-Lin Ho¹, Ming-Yaw Ng¹, Chien Chin Mai², Peng Yu Ko²
and Yia-Chung Chang³

¹Department of Physics, National Cheng Kung University, Tainan 701, Taiwan, Republic of China

²Gamma Optical Co., LTD, Kaohsiung 811, Taiwan, Republic of China

³Research Center for Applied Sciences, Academia Sinica, Taipei 115, Taiwan, Republic of China

E-mail: yiachang@gate.sinica.edu.tw

Received 16 January 2013, in final form 13 February 2013

Published 14 March 2013

Online at stacks.iop.org/JPhysD/46/145106

Abstract

This work introduces the iterative scaling (or inflation) method to systematically approach and analyse the infinite structure of quasi-crystals. The resulting structures preserve local geometric orderings in order to prevent artificial disclination across the boundaries of super-cells, with realistic quasi-crystals coming out under high iteration (infinite super-cell). The method provides an easy way for decorations of quasi-crystalline lattices, and for compact reliefs with a quasi-periodic arrangement to underlying applications. Numerical examples for in-plane and off-plane properties of square-triangle quasi-crystals show fast convergence during iteratively geometric scaling, revealing characteristics that do not appear on regular crystals.

(Some figures may appear in colour only in the online journal)

1. Introduction

Considerable efforts have recently been dedicated to the realization of two- and three-dimensional quasi-crystal structures [1–5], in which the lack of translational symmetry is compensated by rotational symmetries not achievable by conventional periodic crystals, hence providing an alternative route for various applications [6]. The literature shows that quasi-crystals have unusual surface properties such as low coefficients of friction, high hardness and superior wear/corrosion resistance [7]. In addition, quasi-crystals also possess unique switching functionality and flexible compatibility with polymer-dispersed liquid crystals [8, 9]. Inspired by biologic optics, aperiodic structures mimicking subtle and complex surfaces, e.g. butterfly wings or hummingbird feathers, allow us to better imitate and understand nature [10, 11].

Most previous works generate the quasi-crystals by the formal multi-grid method [12], and simulate the properties by super-cell techniques, i.e. a finite segment of the infinite

aperiodic structures, for feasible calculations [13–15]. Since it is not always easy to decide the appropriate segment preserving local geometric orderings near boundaries, this procedure inevitably leads to artificial disclination across super-cells, and thereby consumes high computer resources on larger-size super-cells in order to diminish the influences of these defects (disclinations). Simultaneously the disclinations also prevent the realization of practical manufacture if these super-cell tiles are designed to benefit particular advantages of quasi-crystals. Other works treat the quasi-periodic structure as an irrational cut of hyper-lattices (periodic lattices in a higher dimension than that of the physical space) and can extract the properties of quasi-crystals in the physical space from the single higher-dimensional unit cell [16, 17], hence requiring no super-cell to be sampled. This so-called cut-and-projection method indeed provides an efficient approach to analyse quasi-crystals due to the periodicity of the hyper-lattices, but the high-dimensional acceptance domain functions, e.g. the fractally shaped acceptance domains for the square-triangle tilings [18], could place a curb on the

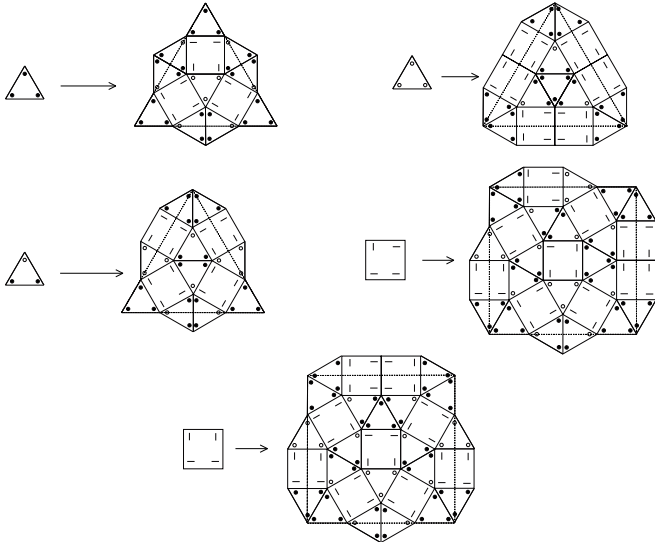


Figure 1. Scaling (inflation) rule by Martin Schlottmann for square-triangle tilings.

accuracy of quasi-crystalline lattices, thus addressing another issue on the compact decoration of lattices for practice applications.

In this work we introduce the iterative scaling (inflation) method developed by E. Harriss, D. Frettlow and others for ‘Tilings Encyclopedia’ [19]. This method can preserve the local geometric orderings across a cell’s boundaries under each iteration if the chosen initial prototype composed of prototiles (tile shapes, see figure 1) already has the orderings. Hence, the structures generated could avoid the issue of artificial disclinations across super-cells. In addition, the action of substitutions for prototiles during the iterative scaling procedure presents a straightforward way to construct compact structures for various applications, e.g. the micro-lens quasi-array. As an example, this work studies quasi-periodic square-triangle structures and analyses the properties of these materials by plane wave expansion (PWE) algorithms [20–22]. Numerical results show good convergence for structures generated by single-iteration or double-iteration scaling, and hence demonstrate a fast and general method to deal with quasi-periodic configurations. The studied example herein finds that (i) the analyses of the in-plane photon transition for quasi-crystal lattices present a significant band-gap structure owing to the rotation-symmetry nature, and can reveal a complete band gap in the mode of cavity; (ii) the analyses of off-plane electromagnetic propagation through micro-lens quasi-arrays shows composite functions comparable to those of regular brightness enhancement films (BEFs) plus diffusers [23]. Simultaneously, the quasi-periodic structure is expected to be immune from unexpected interferences or moires [24, 25] caused among regular periodic patterns.

This paper is organized as follows. Section 2 describes the iterative scaling procedure, and illustrates the atomic decoration of square-triangle quasi-crystals for in-plane analyses and the compact micro-lens with square-triangle arrangement for off-plane studies. This section

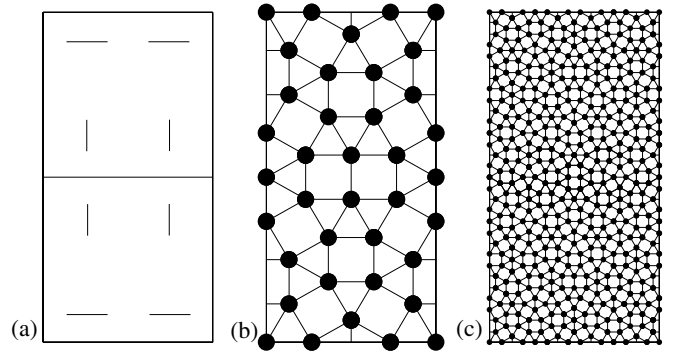


Figure 2. (a) An initial choice of super-cell composed of two square prototiles, (b) the square-triangle structure after single-iteration scaling (with $\zeta = 2 + \sqrt{3}$) and (c) the square-triangle structure after double-iteration scaling (with $\zeta = 2 + \sqrt{3}$). For the square-triangle structure, each lattice site is decorated with an atom having radius r_a , and the length of the edge of square/triangle remains at $r_e = 1/\zeta$.

also reports the refined PWE algorithms. Section 3 is devoted to numerical analyses. Section 4 contains the main conclusions.

2. Theoretical formulae

2.1. Iterative geometric scaling for square-triangle quasi-crystals

Aside from these three-dimensional quasi-crystals with icosahedral symmetry in physical applications, the most relevant are the planar structures with 5-fold (10-fold), 8-fold and 12-fold symmetry. For example, the famous Penrose tilings show statistical 10-fold symmetries [26], and two particular Penrose tilings show global 5-fold dihedral symmetry [27]. The prominent structures with 8-fold symmetry are certainly the Ammann-Beenker tilings [27], whereas those with 12-fold symmetry are the square-triangle tilings. All these three families of the structures above have characteristic building blocks (prototiles) by themselves, and can be generated by an iterative scaling (inflation) method [19]. In fact, the iterative scaling method is given by a set of prototiles T_1, \dots, T_m , a scaling factor ζ , and a rule for how to replace the enlarged prototiles ζT_i with congruent copies of the prototiles.

The first scaling rule yielding square-triangle quasi-periodic structures with 12-fold symmetry was initiated by Schlottmann and is published as a reference [28]. Here, figure 1 shows the scaling rule illustrated by Baake, etc.

In figure 1, the scaling rule had introduced three kinds of triangles and two different kinds of squares, which are distinguished by markings. By iterating the rule for the marked prototiles, one can produce arbitrary large tilings with overlapping parts that are self-similar. For an initial super-cell, which is composed of several prototiles and is chosen to keep local geometric orderings across cells, this self-similarity ensures that scaling-up structures can still preserve the local orderings. Figure 2 illustrates an example for the atomic decoration of square-triangle lattices generated by single- and double-iteration scaling. Here, the local orderings mean that

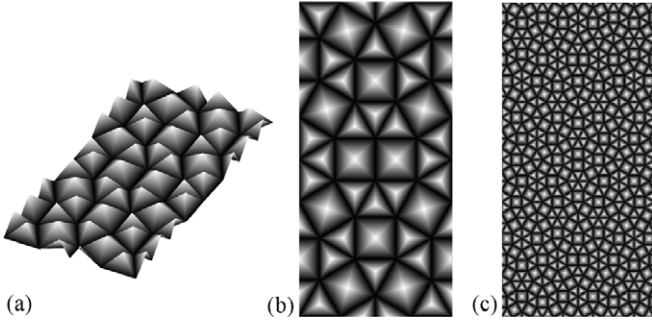


Figure 3. (a) The three-dimensional schematic plot of a compact micro-lens structure in a square-triangle arrangement, (b) profile of a micro-lens structure after single-iteration scaling (with $\zeta = 2 + \sqrt{3}$) and (c) the profile of a micro-lens structures after double-iteration scaling (with $\zeta = 2 + \sqrt{3}$). The length of the edge of square/triangle remains at $r_e = 1/\zeta$.

the tiles remain square or triangle even across the boundaries of cells.

The process of replacing of prototiles further provides an alternative/simple way to construct the compact structure with a quasi-periodic arrangement, e.g. micro-lens configurations, for underlying applications. Figure 3 illustrates an example for compact micro-lens quasi-arrays generated by single- and double-iteration scaling. In this case, the square tiles are stuffed with pyramid while the triangles are stuffed with tetrahedrons.

2.2. PWE method for analyses of in-plane band structure

The Maxwell equation in a transparent, time-invariant, source-free and non-magnetic medium can be written in the following form

$$\frac{1}{\varepsilon(\vec{r})} \nabla \times [\nabla \times \vec{E}(\vec{r})] = \frac{\omega^2}{c^2} \vec{E}(\vec{r}), \quad (1)$$

$$\nabla \times \left[\frac{1}{\varepsilon(\vec{r})} \nabla \times \vec{H}(\vec{r}) \right] = \frac{\omega^2}{c^2} \vec{H}(\vec{r}), \quad (2)$$

where $\varepsilon(\vec{r})$ is the space dependent dielectric function, c is the speed of light in a vacuum, and $\vec{E}(\vec{r})/\vec{H}(\vec{r})$ is the electric/magnetic field vector of a definite frequency ω with time dependence $e^{i\omega t}$. In the cubic lattice structure (of a supercell), the dielectric function term $1/\varepsilon(\vec{r})$ in equations (1) and (2) can be expressed by Fourier expansion

$$\frac{1}{\varepsilon(\vec{r})} = \sum_{\vec{G}} \kappa(\vec{G}) e^{i\vec{G}\cdot\vec{r}}, \quad \varepsilon(\vec{r}) = \sum_{\vec{G}} \varepsilon(\vec{G}) e^{i\vec{G}\cdot\vec{r}} \quad (3)$$

in which $\vec{G} = m\vec{G}_x + n\vec{G}_y + p\vec{G}_z$ is the reciprocal lattice vector ($\vec{R} = m'\vec{\Lambda}_x + n'\vec{\Lambda}_y + p'\vec{\Lambda}_z$ is the lattice vector with relation $G_{i \in \{x,y,z\}} = 2\pi/\Lambda_i$); Otherwise, by the Bloch Theorem, the field vector $\vec{E}(\vec{r})$ and $\vec{H}(\vec{r})$ can be treated as a Fourier series function:

$$\vec{E}(\vec{r}) = \sum_{\vec{G}} \vec{E}(\vec{G}) e^{i(\vec{k}+\vec{G})\cdot\vec{r}}, \quad \vec{H}(\vec{r}) = \sum_{\vec{G}} \vec{H}(\vec{G}) e^{i(\vec{k}+\vec{G})\cdot\vec{r}}, \quad (4)$$

where \vec{k} is the incident wave vector in the first Brillouin zone. Putting equations (3) and (4) into equations (1) and (2) for two-dimensional (x, y) systems results in [20]

$$\sum_{\vec{G}'_{\parallel}} \kappa(\vec{G}_{\parallel} - \vec{G}'_{\parallel}) (\vec{k}_{\parallel} + \vec{G}'_{\parallel}) \cdot (\vec{k}_{\parallel} + \vec{G}'_{\parallel}) \vec{E}_z(\vec{G}'_{\parallel}) = \frac{\omega^2}{c^2} \vec{E}_z(\vec{G}_{\parallel}), \quad (5)$$

$$\sum_{\vec{G}'_{\parallel}} \kappa(\vec{G}_{\parallel} - \vec{G}'_{\parallel}) (\vec{k}_{\parallel} + \vec{G}'_{\parallel}) \cdot (\vec{k}_{\parallel} + \vec{G}'_{\parallel}) \vec{H}_z(\vec{G}'_{\parallel}) = \frac{\omega^2}{c^2} \vec{H}_z(\vec{G}_{\parallel}), \quad (6)$$

where \vec{k}_{\parallel} and \vec{G}_{\parallel} indicate the vectors in the xy plane. Equations (5) and (6) now represent Hermitian eigen-problems, and provide solutions of the band structure with a given \vec{k}_{\parallel} in TE (transverse electric field \vec{E}_z) and TM (transverse magnetic field \vec{H}_z) polarization, respectively.

2.3. Coupled plane-wave method for analyses of off-plane electromagnetic structure

For analyses of off-plane photon propagations, we stratify the three-dimensional geometry into stacks of two-dimensional lattice layers. The individual layer now represents an eigen-system similar to the argument above, but now is globally linked by a boundary matching condition. Consider an off-plane incidence with wave vector \hat{k}_I and polarization vector \hat{u} :

$$\hat{k}_I = k_0 n_I (\sin \theta \cos \varphi \hat{x} + \sin \theta \sin \varphi \hat{y} + \cos \theta \hat{z}), \quad (7)$$

$$\hat{u} = (\cos \psi \cos \theta \cos \varphi - \sin \psi \sin \varphi) \hat{x} + (\cos \psi \cos \theta \sin \varphi + \sin \psi \cos \varphi) \hat{y} - (\cos \psi \sin \theta) \hat{z}, \quad (8)$$

where $k_0 = 2\pi/\lambda$ and λ is the vacuum wavelength of the incident wave. Here, θ is the polar angle and φ is the azimuth angle of \hat{k}_I . The angle between the electric field vector and the incident plane is ψ . Moreover, n_I (n_E) is the refractive index in the incident (exit) layer. Similarly, with Maxwell equations as well as equations (3) and (4), the propagations of \vec{E} fields along the z direction in the ℓ th layer can be formulated as eigen-equations [21]:

$$\begin{bmatrix} \frac{\partial^2}{\partial z^2} \mathbf{E}_{\ell,y}(\vec{G}_{\parallel}) \\ \frac{\partial^2}{\partial z^2} \mathbf{E}_{\ell,x}(\vec{G}_{\parallel}) \end{bmatrix} = \Omega_{\ell} \begin{bmatrix} \mathbf{E}_{\ell,y}(\vec{G}_{\parallel}) \\ \mathbf{E}_{\ell,x}(\vec{G}_{\parallel}) \end{bmatrix}, \quad (9)$$

$$\Omega_{\ell} = \begin{bmatrix} \mathbf{k}_x^2 - \varepsilon_{\ell}(\vec{G}_{\parallel}) + \mathbf{k}_y \kappa_{\ell}(\vec{G}_{\parallel}) \mathbf{k}_y \varepsilon_{\ell}(\vec{G}_{\parallel}) \\ \mathbf{k}_x \kappa_{\ell}(\vec{G}_{\parallel}) \mathbf{k}_y \varepsilon_{\ell}(\vec{G}_{\parallel}) - \mathbf{k}_x \mathbf{k}_y \\ \mathbf{k}_y \kappa_{\ell}(\vec{G}_{\parallel}) \mathbf{k}_x \varepsilon_{\ell}(\vec{G}_{\parallel}) - \mathbf{k}_x \mathbf{k}_y \\ \mathbf{k}_y^2 - \varepsilon_{\ell}(\vec{G}_{\parallel}) + \mathbf{k}_x \kappa_{\ell}(\vec{G}_{\parallel}) \mathbf{k}_x \varepsilon_{\ell}(\vec{G}_{\parallel}) \end{bmatrix}, \quad (10)$$

where \mathbf{k}_x and \mathbf{k}_y are the diagonal matrix with elements $\mathbf{k}_{x,mn} = k_0^{-1}(\vec{k}_I + \vec{G}_{\parallel,mn})_x$ and $\mathbf{k}_{y,mn} = k_0^{-1}(\vec{k}_I + \vec{G}_{\parallel,mn})_y$, respectively. Here, $\vec{G}_{\parallel,mn} = 2\pi m/\Lambda_x \hat{x} + 2\pi n/\Lambda_y \hat{y}$, and $\mathbf{k}_{I,z}$ ($\mathbf{k}_{E,z}$) for the incident (exit) layer is the matrix with diagonal elements $\mathbf{k}_{I(E),zmn} = \sqrt{n_{I(E)}^2 - \mathbf{k}_{x,mn}^2 - \mathbf{k}_{y,mn}^2}$. We can follow up by considering the boundary condition, i.e. matching the tangential electric and magnetic fields at each

interface of nearby layers, for which the governing equation for the transmittance field T and the reflection field R of photons can be derived [21]

$$\begin{aligned} & \begin{bmatrix} u_x \delta_{m0} \delta_{n0} \\ u_y \delta_{m0} \delta_{n0} \\ \delta_{m0} \delta_{n0} (k_{y,00} u_z - n_l \cos \theta u_y) \\ \delta_{m0} \delta_{n0} (n_l \cos \theta u_x - k_{x,00} u_z) \end{bmatrix} + \begin{bmatrix} I & 0 \\ 0 & I \\ \frac{k_x k_y}{k_{l,z}} & \frac{k_y^2 + k_{l,z}^2}{k_{l,z}} \\ \frac{k_x^2 + k_{l,z}^2}{k_{l,z}} & -\frac{k_x k_y}{k_{l,z}} \end{bmatrix} \begin{bmatrix} R_x \\ R_y \end{bmatrix} \\ &= \prod_{\ell} \begin{bmatrix} F_{\ell,11} & F_{\ell,12} X_{\ell} \\ F_{\ell,21} & F_{\ell,22} X_{\ell} \\ F_{\ell,31} & F_{\ell,32} X_{\ell} \\ F_{\ell,41} & F_{\ell,42} X_{\ell} \end{bmatrix} \begin{bmatrix} F_{\ell,11} X_{\ell} & F_{\ell,12} \\ F_{\ell,21} X_{\ell} & F_{\ell,22} \\ F_{\ell,31} X_{\ell} & F_{\ell,32} \\ F_{\ell,41} X_{\ell} & F_{\ell,42} \end{bmatrix}^{-1} \\ & \times \begin{bmatrix} I & 0 \\ 0 & I \\ -\frac{k_x k_y}{k_{E,z}} & -\frac{k_y^2 + k_{E,z}^2}{k_{E,z}} \\ \frac{k_x^2 + k_{E,z}^2}{k_{E,z}} & \frac{k_x k_y}{k_{E,z}} \end{bmatrix} \begin{bmatrix} T_x \\ T_y \end{bmatrix}, \quad (11) \end{aligned}$$

where X_{ℓ} is a diagonal matrix with diagonal elements equal to $X_{\ell,i} = \exp[-k_0 \sigma_{\ell,i} z_{\ell}]$. Here, z_{ℓ} is the thickness of ℓ_{th} layer; $\sigma_{\ell,i}$ are the elements of Υ_{ℓ} , a diagonal matrix of the positive square roots of the eigenvalues of Ω_{ℓ} ; $F_{\ell,11} = F_{\ell,12} = W_{\ell,2}$, $F_{\ell,21} = F_{\ell,22} = W_{\ell,1}$, $F_{\ell,31} = iV_{\ell,2}$, $F_{\ell,32} = -iV_{\ell,2}$, $F_{\ell,41} = iV_{\ell,1}$, and $F_{\ell,42} = -iV_{\ell,1}$. We denote the eigenvector matrix of Ω_{ℓ} as $W_{\ell} = [W_{\ell,1} \ W_{\ell,2}]^T$, and $V_{\ell,i}$ is defined by

$$V_{\ell,1} = [k_x k_y W_{\ell,1} + (\varepsilon_{\ell} - k_y^2) W_{\ell,2}] \Upsilon_{\ell}^{-1}, \quad (12)$$

$$V_{\ell,2} = [(k_x^2 - \varepsilon_{\ell}) W_{\ell,1} - k_x k_y W_{\ell,2}] \Upsilon_{\ell}^{-1}. \quad (13)$$

By solving the eigen-equations (9)–(10) for each layer and continuing with the boundary-matching equation (11), the transmittance field T and the reflection field R of photons through the systems can be decided. An enhanced approach to improving the numerical stability for solving equation (11) is noted in [29].

3. Numerical analyses

3.1. Band-Gap structure of square-triangle quasi-crystals

In this subsection, we compute the photonic band structure for square-triangle quasi-crystals by conventional PWE calculation. Here, the increasingly accurate approximants (super-cells) in figure 2 are generated by iterating the scaling rule to ensure the local orderings across cells and hence to enhance the efficiency of convergence. For illustration, we assume the materials are composed of the insertion ($\varepsilon_a = 8.9$) and air ($\varepsilon_a = 1.0$) for the photonic quasi-crystals, while they are composed of the insertion ($\varepsilon_a = 1.0$) and air ($\varepsilon_a = 8.9$) for the photonic cavity. Numerical simulations include $4^2 \times N_a$ plane waves to achieve convergence accuracy, where N_a represents the number of atoms. We perform most of the band-structure calculations around a contour along the first Brillouin zone of the respective system, which includes the high-symmetry k -space points, $\Gamma = 0$, $X = \vec{G}_x/2$, $M = (\vec{G}_x + \vec{G}_y)/2$ and $Y = \vec{G}_y/2$.

Figure 4 displays two TE photonic band gaps with $\Delta\omega/\omega_c = 23\%$ for the upper one and $\Delta\omega/\omega_c = 32\%$ for the

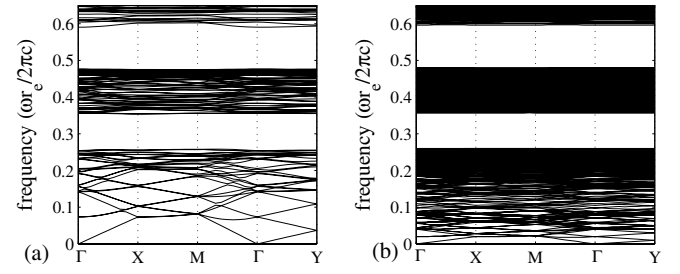


Figure 4. (a) Band-gap structure of square-triangle quasi-crystals of figure 2(b) with atomic size $r_a = 0.09$ ($r_e = 1/\zeta$) in TE polarization, and (b) band-gap structure of square-triangle quasi-crystals of figure 2(c) with atomic size $r_a = 0.09$ ($r_e = 1/\zeta$) in TE polarization.

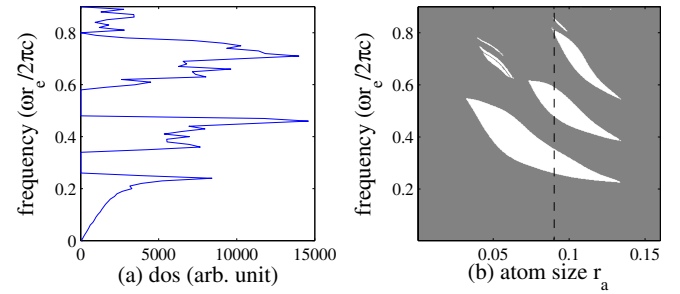


Figure 5. (a) Density of state (DOS) of square-triangle quasi-crystals of figure 2(b) with atomic size $r_a = 0.09$ ($r_e = 1/\zeta$) in TE polarization and (b) diagrams of band-gap structure as a function of atom size (r_a), in which the grey regions represent the allowed bands and the dash line indicates atom size $r_a = 0.09$ ($r_e = 1/\zeta$).

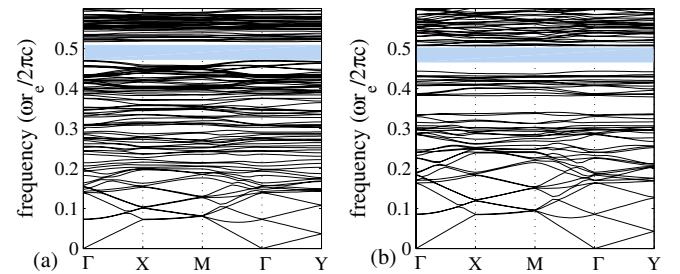


Figure 6. Complete band gap of square-triangle quasi-crystal cavity. Figure (a) shows the band structure in TE polarization and figure (b) shows the band structure in TM polarization with $r_a = 0.11$, $r_e = 1/\zeta$, $\varepsilon_a = 1.0$ and $\varepsilon_b = 8.9$.

lower one, where ω_c is the gap central frequency. Numerical results show fast convergence since the band gap remains stable while the size of the super-cell scales up by $\zeta^2 \simeq 14$ times (from figures 2(b) to (c)). As a check, we perform an alternative calculation of density of states (DOS), i.e. calculate all k -points with grid interval $dG_{i \in \{x,y\}} = 2\pi \cdot 0.025/\Delta_i$ in the first Brillouin zone, as in figure 5(a), and obtain results on the TE band gap that are completely consistent. Figure 5(b) presents the study of atom-size dependence (with constant prototiles $r_e = 1/\zeta$). Results indicate that, with given materials, the optimal structure of square-triangle quasi-crystals can have a band gap of $\Delta\omega/\omega_c \simeq 50\%$ at $r_a = 0.06$ (with $r_e = 1/\zeta$).

For the complete band gap, i.e. frequency ranges over which electromagnetic wave propagation is prohibited for all directions and polarizations, figure 6 illustrates an investigation on the photonic quasi-crystal cavity with square-triangle

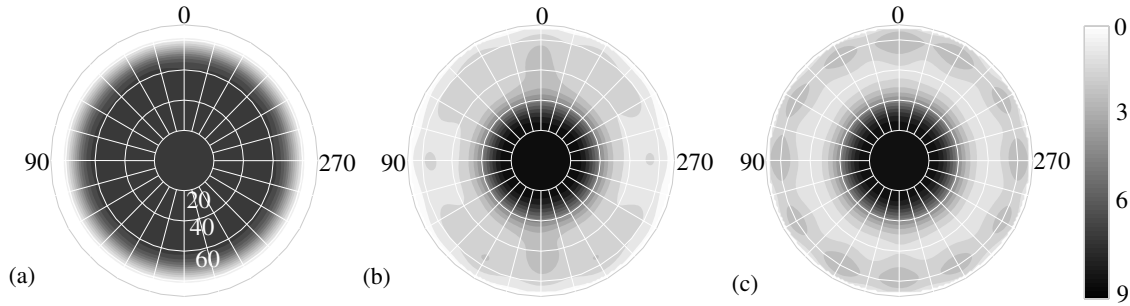


Figure 7. Polar iso-candela plots for (a) emerged photons from flat structures without micro-lens, (b) emerged photons from micro-lens quasi-arrays of figure 3(b) with $r_e = 20/\zeta \simeq 5.36 \mu\text{m}$, and (c) emerged photons from micro-lens quasi-arrays of figure 3(c) with $r_e = 20/\zeta \simeq 5.36 \mu\text{m}$. The height of micro-lens is $2.5 \mu\text{m}$ and the refractive index is 1.5 for $\lambda = 0.55 \mu\text{m}$.

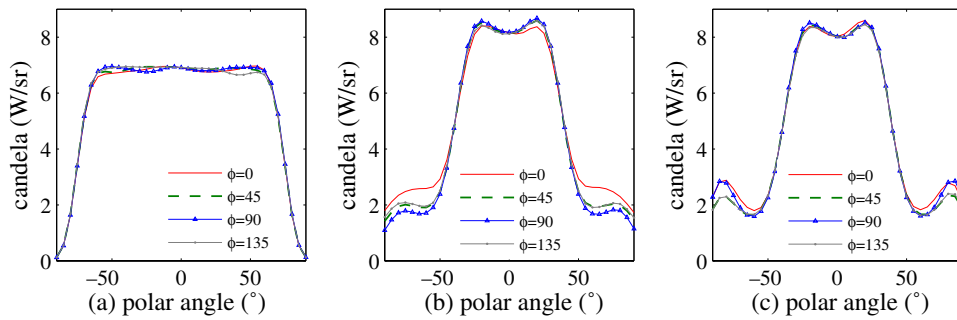


Figure 8. Cross section views corresponding to figure 7 at different azimuthal angles: $\phi = 0^\circ, 45^\circ, 90^\circ$ and 135° .

arrangement (figure 2(b) with $\epsilon_a = 1.0$ and $\epsilon_b = 8.9$). Exploring the result shows that there exists a band gap of $\Delta\omega/\omega_c = 7\%$ in both TE and TM polarizations. Further works will investigate the underlying synergetic interplay between Bragg resonances and Mie resonances [30].

3.2. Optics of micro-lens quasi-array

Instead of traditional optic devices with regular compact periodic structures, it is feasible to explore the quasi-periodic structure for underlying applications, e.g. composite optical functions. Basically, the quasi-periodic structure presents several intrinsic features: (i) with long-range orientation ordering, it could lead to rotational-symmetric optical characteristics, (ii) with short-range geometric ordering, it could reserve the functions of traditional optic systems, (iii) with a partial random nature, it could prevent unexpected interferences or moires [24, 25] caused among regular periodic patterns.

This work investigates the micro-lens with a square-triangle arrangement as shown in figure 3 for light-condensing optics. We compute numerical simulations by coupled plane-wave algorithms as done above. Relevant parameters are given as the edge length of a square or triangle tile is $r_e = 20/\zeta \simeq 5.36 \mu\text{m}$, the height of micro-lens (the height of pyramid in a square tile and the height of tetrahedron in a triangle tile) is $2.5 \mu\text{m}$ and the refractive index of materials is 1.5 at a wavelength of incidence $\lambda = 0.55 \mu\text{m}$. Figures 7 and 8 present the results of calculations. Figure 7(a) displays the angular shape of the intensity of the incidence. Its cross-section is viewed at different azimuthal angles $\phi = 0^\circ, 45^\circ, 90^\circ$ and 135° , numerically illustrated in

figure 8(a). Figures 7(b) and (c) show the angular shape of intensity of emerged photons from micro-lens quasi-arrays for the single-iteration and double-iteration scaling structures (figures 3(b) and 3(c)), respectively. Figures 8(b) and (c) numerically depict the corresponding cross-section views as well. Numerical calculations indicate evident/convergent results for the efficiency of photon-condensing along the normal direction, although there exists a finite deviation on the wide-angle transmittance between different iterating structures. We find that the micro-lens quasi-array indeed exhibits composite functions comparable to that of regular BEFs plus diffusers [23].

4. Conclusions

This work introduces the iterative scaling (inflation) method to quickly analyse quasi-periodic structures for various applications. Studies of example cases on square-triangle configurations demonstrate an easy way to construct quasi-periodic materials, e.g. photonic quasi-crystals and micro-lens quasi-arrays. Numerical calculations show fast convergence for inspecting the properties of structures proceeding only with single-iteration scaling. Analytic results present noticeable characteristics for the band structures of quasi-crystals as well as the composite functions of micro-lens, and provide an alternative opinion on designs for future applications.

Acknowledgments

This research was funded by the National Science Council of Taiwan under Contract Nos NSC 100-2811-M-001-100

and NSC 101-2112-M-001-024-MY3, and support of National Center for Theoretical Science (South) is gratefully acknowledged.

References

- [1] Shir D, Liao H, Jeon S, Xiao D, Johnson H T, Bogart G R, Bogart K H A and Rogers J A 2008 *Nano Lett.* **8** 2236
- [2] Zito G, Piccirillo B, Santamato E, Marino A, Tkachenko V and Abbate G 2008 *Opt. Express* **16** 5164
- [3] Yeo J B, Yun S D, Kim N H and Lee H Y 2009 *J. Vac. Sci. Technol. B* **27** 1886
- [4] Yang Y, Zhang S and Wang G P 2006 *Appl. Phys. Lett.* **88** 251104
- [5] Guo M, Xu Z and Wang X 2008 *Langmuir* **24** 2740
- [6] Charlton M D B, Zoorob M E and Lee T 2007 *Proc. SPIE* **6486** 64860R
- [7] Dubois J M 1993 *Phys. Scr.* **T49** 17
- [8] Gorkhali S P, Qi J and Crawford G P 2005 *Appl. Phys. Lett.* **86** 011110
- [9] Gorkhali S P, Crawford G P and Qi J 2005 *Mol. Cryst. Liq. Cryst.* **433** 297
- [10] Lee L P and Szema R 2005 *Science* **310** 1148
- [11] Huang J, Wang X and Wang Z L 2006 *Nano Lett.* **6** 2325
- [12] Janot C 1997 *Quasicrystals: A Primer* (Oxford: Oxford University Press)
- [13] Villa A D, Galdi V, Capolino F, Pierro V, Enoch S and Tayeb G 2006 *IEEE Antennas Wireless Propag. Lett.* **5** 331
- [14] Kaliteevski M A, Brand S, Abram R A, Krauss T F, DeLa Rue R M and Millar P 2000 *J. Mod. Opt.* **47** 1771
- [15] Florescu M, Torquato S and Steinhardt P J 2009 *Phys. Rev. B* **80** 155112
- [16] Rodriguez A W, McCauley A P, Avniel Y and Johnson S G 2008 *Phys. Rev. B* **77** 104201
- [17] Ho I L, Lee M T and Chang Y C 2012 *J. Opt. Soc. Am. B* **29** 382
- [18] Baake M, Klitzing R and Schlottmann M 1992 *Physica A* **191** 554
- [19] online available: <http://tilings.math.uni-bielefeld.de/>
- [20] Ho K M, Chan C T and Souloulis C M 1990 *Phys. Rev. Lett.* **65** 3152
- [21] Moharam M G, Pommet D A and Grann E B 1995 *J. Opt. Doc. Am. A* **12** 1077
- [22] Ho I L, Chang Y C, Huang C H and Li W Y 2011 *Liq. Cryst.* **38** 241
- [23] Joo B Y and Shin D H 2010 *Displays* **31** 87
- [24] Amidror I 2000 *The Theory of the Moiré Phenomenon* (London: Springer)
- [25] Ho I L, Wang T C, Chang Y C and Li W Y 2012 *Appl. Opt.* **51** 5806
- [26] Frettlow D 2008 *Philo. Mag.* **88** 2033
- [27] Grunbaum B and Shephard G C 1987 *Tilings and Patterns* (New York: Freeman)
- [28] Hermisson J, Richard C and Baake M 1997 *J. Physique I* **7** 1003
- [29] Moharam M G, Pommet D A and Grann E B 1995 *J. Opt. Doc. Am. A* **12** 1077
- [30] John S and Wang J 1991 *Phys. Rev. B* **43** 12772